EUROPEAN LABORATORY FOR PARTICLE PHYSICS

CERN-EP/98-XXX
April 28th, 1998

Thin Scintillating Tiles with High Light Yield for the OPAL Endcaps

Abstract

Arrays of thin scintillating tiles with embedded wavelength shifting fibre readout have been installed in the OPAL endcaps to improve trigger performance, time resolution and hermeticity for experiments at LEP II. The arrays were required to have high single particle detection efficiency, uniform response, low noise and good time resolution. Limited space for the detector, and a strong magnetic field in the endcap region, resulted in a need for high light output per unit thickness of scintillator, and remote readout. In addition, because of limited space for readout cables, a high light yield per embedded fibre was required. This paper describes the design and construction of a tile array that satisfies these requirements. A light yield of 14 photoelectrons per minimum ionizing particle and a time resolution of 3 ns were obtained during 1997 LEP operation.

Submitted to Nucl. Inst. and Meth.

G. Aguillion[5], B. Anderson[11], D. J. Attree[11], A. H. Ball[8], R. Bard[8], S. Bentvelsen[5], S. T. Betts[11], M. Boutemeur[9], B. Caron[1], A. Charalambous[11], J. P. Chatelain[5], J. Colmer[8], P. Courarie[5], M. Cresswell[11], R. Davis[1], J. Dumper[11], A. Faust[1], D. Fong[8], T. J. Fraser[11], M. Garza[8], D. M. Gingrich[1], R. Gollay[11], M. Guillot[5], L. Holm[1], D. Horváth[4], F. Jacob[10], P. I. Kayal[1], S. Lautenschlager[6], A. L. Macpherson[1], J. P. Martin[9], W. J. McDonald[1], D. J. Miller[11], W. Miller[8], S. Mullin[1], G. Pásztor[4], J. L. Pinfold[1], L. del Pozo[5], H. Przysiezniak[1], A. Renoux[5], N. L. Rodning[1], Y. Rozen[5], L. Schaffer[8], J. Schieck[7], C. Selby[3], K. Smith[11], W. Springer[1], F. Strumia[2], S. di Vincenzo[5], L. Wampler[1], P. S. Wells[5].

[1]Centre for Subatomic Research, Physics Department, Univ. of Alberta, Edmonton Ab. T6G 2N5 Canada

[2]Dipartimento di Fisica, Univ. di Bologna, Vitale Berti Pichat 6-2 I-40127 Bologna, It.

[3]Brunel University, Uxbridge, Middx. UB8 3PH UK.

[4]Research Institute for Particle and Nuclear physics, H-1525 Budapest, Hungary.

[5]CERN CH-1211, Geneva 23, Switzerland

[6]Duke Univ., Department of Physics, P.O. Box 90305, Durham, NC 27708-0305 U.S.A.

[7]Physikalsiches Inst., Univ Heidelberg, Philosophenweg 12-D69120, Heidelberg, Germany

[8]University of Maryland, Physics Department, College Park, Maryland 20742 U.S.A.

[9]Laboratoiré de Physique Nucleairé, Université de Montréal, Case Postale 6128 Succursale 'A' Montréal, Que. H3C 3J7 Canada

[10]Rutherford Appleton Laboratory, Chilton, Didcot, Oxon, OX11 0QX U.K.

[11]University College London, Physics Department, London, WC1E 6BT U.K.

1 Introduction and Motivation

The OPAL detector [1] at LEP has been improved for use at higher collision energies, by installing scintillating tile layers (denoted TE and MIP plug) in the endcaps, as shown in fig. 1.

The TE scintillators, which complement existing detectors in the barrel region, efficiently detect charged particles or converted photons, with good time resolution. The TE information provides a time reference for interpreting signals from slower sub-detectors and is used in conjunction with them to construct more robust and selective track triggers. A particular case is the endcap electromagnetic calorimeter, where isolated clusters with no associated charged particle track (photon candidates) may otherwise be faked by out-of-time tracks, such as cosmic rays. Closer to the beam pipe, the MIP plug scintillators extend the angular range for detecting minimum ionizing particle (MIP) tracks from the 200 mrad limit of the poletip hadron calorimeter to 43 mrad. In this angular range, the existing system of small angle calorimeters is sensitive only to electrons and photons.

In contrast with earlier LEP studies at the Z^0 resonance, the ongoing program at LEP II is characterized by low cross-sections, with an emphasis on new particle searches. Amongst the important signatures for new physics are final states with unbalanced visible momentum, or those containing isolated photons. The efficiency, hermeticity and time resolution of the new scintillator system improve performance in both cases. The MIP plug also provides a trigger for certain 2-photon processes.

High luminosity is being delivered by operating the LEP accelerator with high beam currents, often using a multi-bunch structure. Machine-related backgrounds generally increase with both current and collision energy, while collision intervals reduce from 22 μs to a few hundred ns when multiple bunches are used. The precise timing information from the new scintillators improves background rejection in the endcap region and simplifies the unambiguous determination of the collision time.

The following sections describe the design, construction and performance of the scintillating tile system, some aspects of which have been previously presented elsewhere [2].

2 Constraints

The essential requirements for the scintillating tile arrays were high and uniform light yield, low noise and a time resolution of $\leq$ 5 ns, which is sufficient to efficiently identify halo muons or cosmic rays passsing through both endcaps (5 m separation) and to reject any hits caused by excitation of clear fibres by incoming particle bunches. (flight path difference of 2 $\times$ 2.5 m). Low construction cost, low maintenance and high reliability were also important, the latter because of infrequent access opportunities. The physical constraints were the limited ($\sim$20 mm) thickness obtainable by displacing existing detectors, the restricted volume of cables which can exit the endcap, the 0.4 T magnetic field and the required solid angle coverage. In the angular range 318 to 609 mrad ($\cos\theta = 0.95$ to 0.82), the TE tile system (see fig 1) has to overlap with the existing barrel scintillators and extend down to the limit of tracking. Maximum hermeticity is needed in the MIP plug region below the 200 mrad limit of MIP detection by the poletip hadron calorimeter.

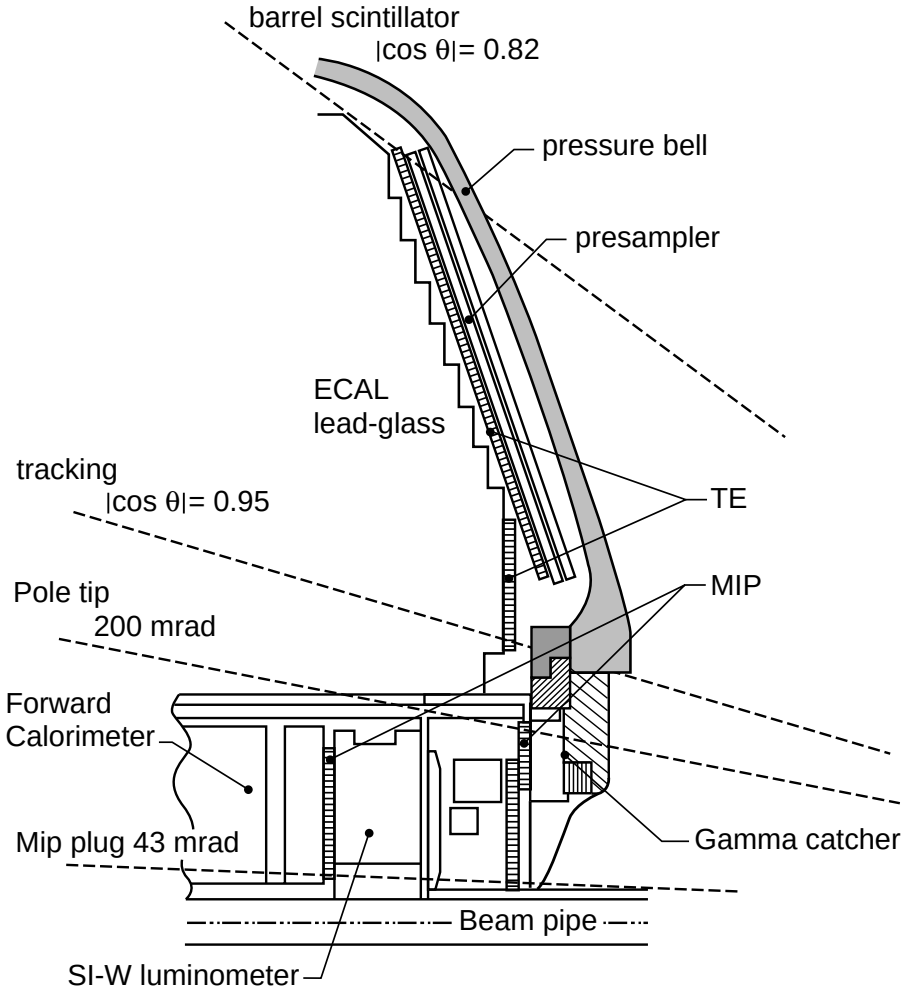

Figure 1: Position of the Tile Endcap (TE) and MIP Plug relative to the beam pipe, pressure bell, presampler and lead glass energy calorimeter (ECAL). The dashed lines represent particle trajectories at the limits of polar angle coverage by various OPAL subdetectors. The e^+e^- interaction point where the dashed lines converge is approximately 2.5 m to the right of the center of the figure and the outer radius of the largest TE tile sector is 1750 mm.

Thus no azimuthal dead-space and very little radial dead-space could be left within the total available volume, ruling out the use of conventional light guides or local readout. The only practical solution was to use tiles, with embedded wavelength shifting (WLS) fibres, coupled by clear fibres to remote photo-transducers outside the endcap. Here the magnetic field is low enough for conventional photomultipliers to operate (with magnetic shielding). The restricted total volume of clear fibres means that a high light yield per embedded fibre is needed.

3 Tile-Fibre Technique

The technology of scintillator tiles read out by embedded wavelength-shifting fibres was first developed for the UA1 experiment and at Protvino [3]. It was extensively studied and refined by the SDC collaboration for both electromagnetic and hadronic calorimetry [4] and is installed in the upgraded CDF endplug [5]. Both ATLAS and CMS collaborations at LHC are planning to use the tile-fibre technique in their hadron calorimeters and further extensive research and development programs have been undertaken [6]. In these large scale applications for calorimetry, the light yield requirements per tile are relatively modest. Several detectors have been built to achieve single layer efficiency for MIPS, amongst which are the SCITIL for the WA89 SPACAL calorimeter [7], the ZEUS FCAL/RCAL presampler [8], the Delphi luminosity detector photon veto [9] and the D0 muon upgrade [10]. In our case, the light yield requirements are particularly challenging, in view of the constraints described above as well as the need to guarantee high efficiency of all channels for a MIP, and to optimize the time-resolution of relatively large tiles.

4 Optimization of Light-Yield

The light yield of tile-fibre combinations has been extensively studied [5, 11, 12, 13] and shown to be roughly proportional to tile thickness, fibre diameter and the length of WLS fibre within the tile per unit area. The shape, depth and polish of the fibre groove were also found to be important parameters. The number of separate fibre grooves which are needed and the optimum number of fibres per groove depend on the tile and fibre dimensions, the uniformity of response required, and the attenuation characteristics of the scintillator and WLS fibre. Some authors have noted that installing two fibres in a single groove can work as well as putting each in a separate groove (see for example [11, 13]). The use of optical glue to hold the fibre in place improves the light collection and relaxes the machining tolerances, at the expense of complicating the assembly and introducing more risk of long-term deterioration.

In order to optimize the light yield for our application, we have studied a number of tile-fibre configurations using a combination of simulations and test measurements [14, 15]. The techniques used and the results obtained are summarized below.

4.1 Simulation

Full Monte Carlo simulation of light collection from a complex tile-fibre detector requires a large amount of computer time. Analytical calculations are more efficient and work well for simple geometries, but are not practical for complex ones. To understand the main parameters affecting light yield and uniformity, a simple technique was evolved, similar to that described in ref. [16], which combines the best features of the Monte Carlo and analytic approaches and can simulate arbitrarily complicated geometries.

The light yield calculation was factorized into three parts: the transport of scintillation photons to an absorption point in a WLS fibre, the transport of re-emitted (wavelength shifted) photons through the WLS fibre, connector and clear fibre and finally, the photoelectron emission and amplification within the photomultiplier tube. The first is important

for simulating the uniformity of response. All three contribute to the simulation of the amplitude and time structure of the final photomultiplier signal. For complex geometries, photon pathways from an origin in the scintillator to intersection of a WLS fibre, including reflections from scintillator faces or wrapping, were obtained from GEANT [17] ray tracing, assuming no reflection or transmission losses. The probability that a photon was actually absorbed by the WLS fibre was then determined analytically by applying suitably chosen attenuation, transmission and absorption coefficients to the photon path. Photons re-emitted in the WLS were assumed to be trapped if they satisfied a trapping condition which depends on the refractive indices of the fibre core and claddings, and on the radius and angle of emission at the point of emission [18]. Subsequent propagation of a trapped photon through WLS, connector and clear fibre depends mainly on the distance travelled between the absorption/re-emission point and the photocathode. All effects that influence the attenuation of photons, such as connectors, couplers and transport in the WLS and clear fibres were accounted for by applying suitable attenuation coefficients, some of which depend on the angle and radius of re-emission.

The number of photoelectrons emitted from the photocathode, and their time distribution was obtained from the simulated intensity and time distribution of photons arriving at the photomultiplier and the quantum efficiency of the cathode. The time resolution of the detector was then obtained as a function of integration time constant and discriminator threshold using the known single electron response of the photomultiplier tube. After tuning to results from test tiles (see 4.2), the simulation was able to correctly predict the light-yield, uniformity and time resolution of complex geometries, enabling the final design to be optimized without building multiple prototypes.

4.2 Light Yield Tests

Tests were conducted to determine light yields from a set of 10 mm thick 300 mm square tiles of BC408 scintillator [19] each with 1.8 m of embedded 1 mm diameter Y11 200 non-S WLS fibre [20]. The tiles had a variety of groove patterns and various polishing and wrapping techniques were used. One or both ends of the embedded WLS fibres were coupled either directly, or via connectors and clear fibre, to a photomultiplier. Light yields and uniformity were observed using a cosmic ray track reconstruction telescope and a collimated Ru source mounted on an x-y scanner. ^{106}Ru decays via ^{106}Rh producing 3.5 MeV electrons which simulate minimum ionizing particles fairly well. Observed cosmic ray charged signal distributions (corrected to normal incidence) were fitted to obtain the mean number of photoelectrons n_{pe}, using a Poisson distribution convoluted with a Gaussian single photon resolution function. The photoelectron yield was checked by probing the single photoelectron response of the photomultiplier using a progressively attenuated LED and also by checking the proportion of events with zero counts.

For tiles of this size, with diamond milled edges, and wrapped in Tyvek 1073D [21], it was found that the best uniformity comes from grooves evenly distributed over the tile surface, typically leaving no point more than 50mm from a groove. Inserting two fibres in a deeper groove was almost as effective in increasing light output as doubling the number of grooves containing single fibres. It was also noted that coupling both ends of each fibre to the photomultiplier improves time resolution, avoids the need for mirroring, and

allows easy and thorough pre-testing of the WLS/connector assemblies before gluing into the scintillator tiles. In this way, expensive tile wastage due to faulty WLS fibres can be avoided.

Additional tests were conducted using tiles with differing shape, groove geometry and surface treatment. Observed and simulated light yields were compared and the results used to tune parameters of the simulation. Once this was done, the simulation was able to correctly predict the response of both simple and complicated tile-fibre combinations. It was concluded that the best arrangement for satisfying the requirements of high light yield with good uniformity and time resolution has diamond milled grooves on both sides of the tile, with complementary groove patterns following sinusoidal paths to increase embedded fibre length and with two WLS fibres per groove.

5 Detailed Design

5.1 Tiles

The scintillator tiles in each endcap are arranged in sectors as shown in figs. 2 and 3.

Subdivision of the outer part of TE into 48 sectors was mandated by the mechanical requirement of installation beneath the 16 sector presampler detector (PE) and by the 24-fold azimuthal segmentation of the OPAL trigger logic. At least 2 separate scintillator elements per sector were needed to match the truncated cone shape of the electromagnetic calorimeter, ECAL, and in practice, the larger of these was divided in two because of the limited size of precision thickness grooved scintillators that could be supplied. To economize on photomultiplier channels, the light output from tiles in the same outer 1/24 sector are grouped together on the same photomultiplier. The inner 1/24 sectors, which do not conflict with PE, are single piece tiles. Each of these is read out by separate photomultipliers, allowing for disconnection of the inner sectors from the trigger in case of high background rates caused by their proximity to the beamline.

For the MIP Plug, the tile layout is dictated by manufacturing simplicity, the need to cover the required angular regions with at least a two-fold coincidence of approximately annular layers, by the azimuthal subdivision needed for trigger and veto functions and by the high beam-induced backgrounds expected. The tiles are arranged as an inner and an outer pair of annular layers, each divided into 8 tile sectors. The two outermost layers are grouped in a single assembly, separated by a 4 mm layer of lead to reduce background from synchrotron photons. Each layer is readout as four two-tile quadrants. The two inner layers lie within the fiducial angular range of the luminosity calorimeters, where material must be minimized. Protection from background coincidences is achieved in this case by placing the layers on either side of the support structure of the silicon-tungsten luminometer, and by reading out individual sector elements.

In total therefore, there are 120 TE tiles and 32 MIP plug tiles in each endcap. All are 10 mm thick and they vary in area from 470 to 900 cm^2. The tiles and other optical components were chosen to optimize the collection of scintillation photons ($\lambda \sim 420$ nm) in the WLS fibre, and transmission of the wavelength shifted light ($\lambda \sim 500$ nm) around the peak sensitivity of the photomultiplier.

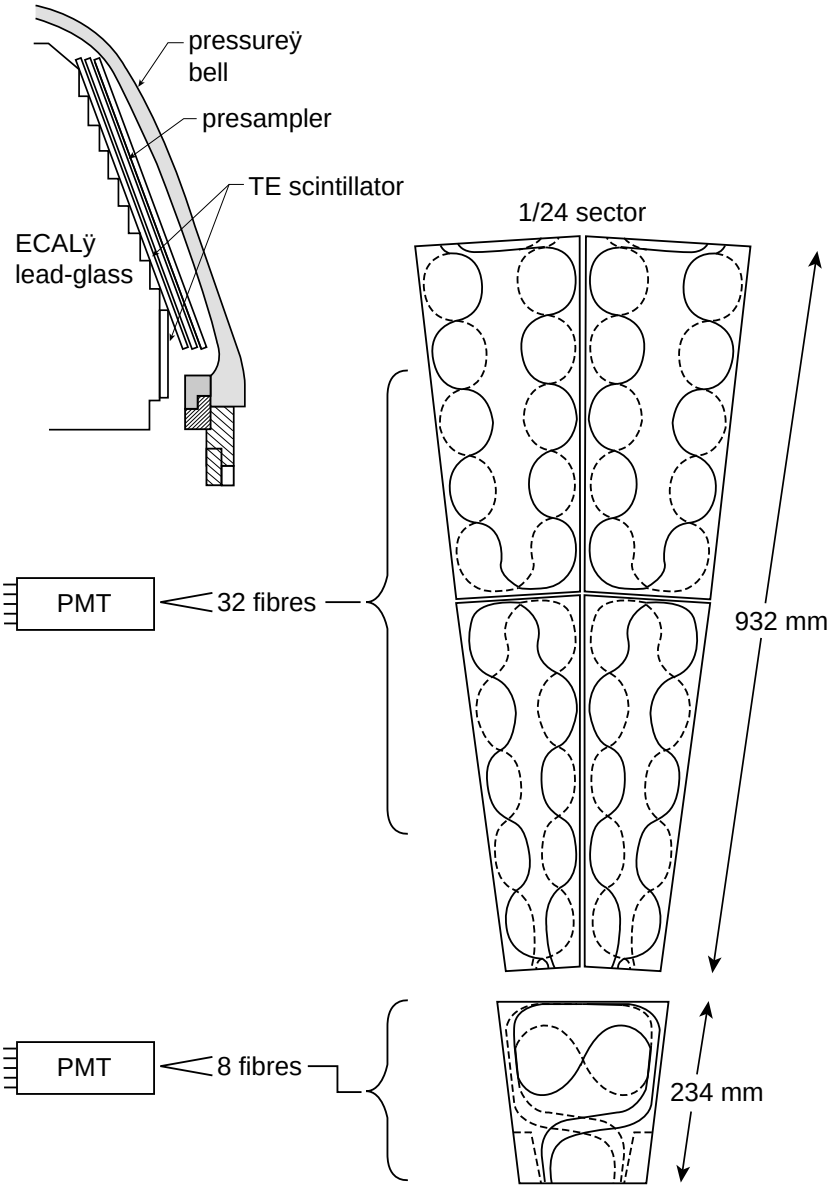

Figure 2: TE Sector arrangement

The tiles were made of BC408 scintillator [19] of refractive index $n_{scint} = 1.58$, with the groove patterns shown in fig. 2 and fig. 3 diamond milled on both sides of the tile, following a complementary tool path. BC408 scintillator was chosen because it gave acceptable light yield (when matched with all the other components) combined with reasonable durability, availability and cost. In addition, the supplier was willing to develop the milling and quality control techniques required to reliably produce complex groove paths. The layout of the WLS fibre grooves within the tile was chosen to maximize embedded fibre length, while respecting the lower limit of 40 mm on WLS fibre bending radius and distributing the groove pattern uniformly over the tile surface. This layout

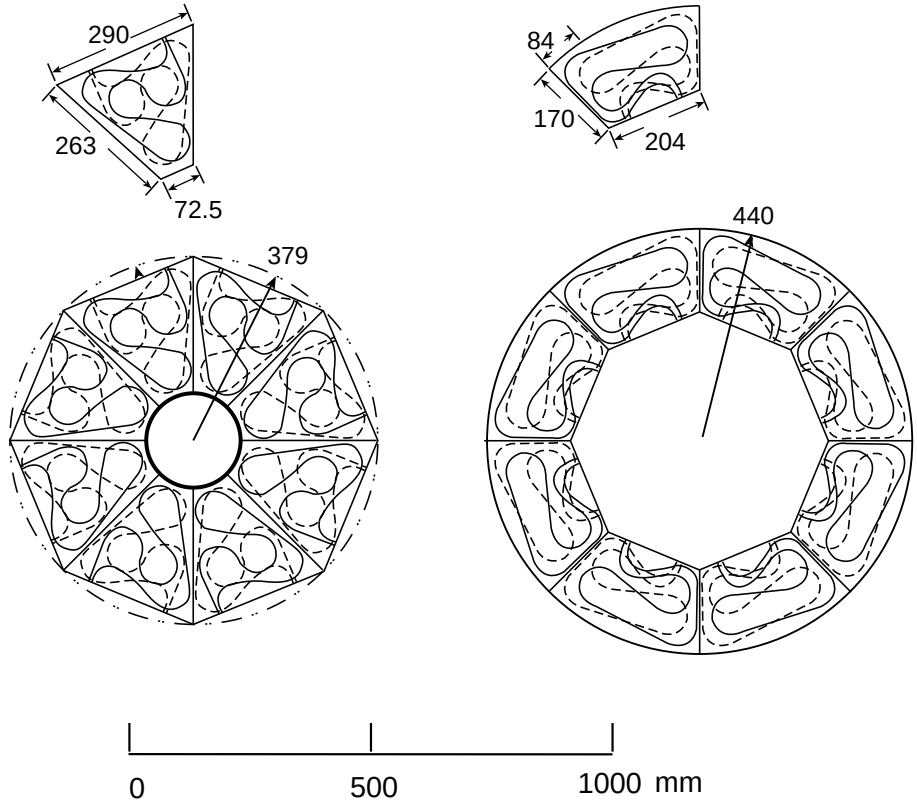

Figure 3: MIP Plug Sector arrangement showing inner and outer layers

resulted in a ratio of embedded length to area of approximately 0.09 cm^{-1} for our tiles.

5.2 WLS and Clear fibres

Double-clad WLS fibres were chosen to maximize light output. The types used were Kuraray Y11-200 non-S [20], and Bicron BCF91a mc [19]. Both have an inner core of polystyrene, with $n_{wlscore} = 1.6$ and successive cladding layers of polymethyl methacrylate (PMMA) and fluorinated PMMA ($n_{wlscladding} = 1.49$ and 1.42 respectively). The absorption spectra of these WLS fibres are a reasonable match to the BC408 scintillator output. In addition, the emitted wavelength spectrum is well transmitted by the chosen clear fibre, within the sensitive range covered by several commercially available photomultiplier tubes with 'green-extended' cathodes.

WLS 'looms' were constructed by gluing the WLS fibre ends into precision optical connectors (see section 5.3) on plastic jigs replicating exactly the final scintillator and connector positions as well as the scintillator groove pattern. NE581[22] or BC 600 [19] optical cement was used. The ends of the fibres were fly-cut, then polished using Novus type 2 polishing compound [23] to produce optically flat surfaces. Pre-assembly of these WLS 'looms' allowed the fibres to be tested in their connectors before being glued into the scintillator.

The 1 mm diameter clear fibres are Hoechst Infolite ER51 [24], a singly clad fibre with $n_{clearcore} = 1.49$ and $n_{clearcladding} = 1.42$. This was selected for low attenuation (120dB/km at 500 nm) and a thin, light-tight polyethylene outer jacket, giving an overall diameter of 1.5 mm, small enough to permit packing sufficient fibres in the available space for exit from the endcaps. For the tiles around the beam pipe, Mitsubishi SH4001-16 [25] with overall diameter 1.6 mm and otherwise identical properties, was substituted. Losses at the connector due to the poor match between the core refractive indices of the WLS and clear fibres are more than compensated by the much lower attenuation in the clear fibre of wavelengths near the peak sensitivity of the photomultiplier tube.

Clear fibres were cut to appropriate length and then glued into connectors in groups of four, polished and pre-tested. After this, looms were completed by gluing the free ends of up to eight such groups into a coupler (described in section 5.4), which was designed to mate directly to the window of a photomultiplier tube. The clear fibre looms carry the light up to 15m, from the edges of the active detector inside the endcap, to the photomultiplier tubes, which are mounted in accessible housings, outside the region of high magnetic field.

5.3 Connectors

Existing commercially available optical connectors [26] were too large and unsuitable for mounting on the tile sector baseplates (see section 6.2). An inexpensive custom-design, based on similar principles, was machined from Delrin [18] plastic and provides for stable, repeatable alignment of the fibres to 10 μm with a surface flatness of a few microns.

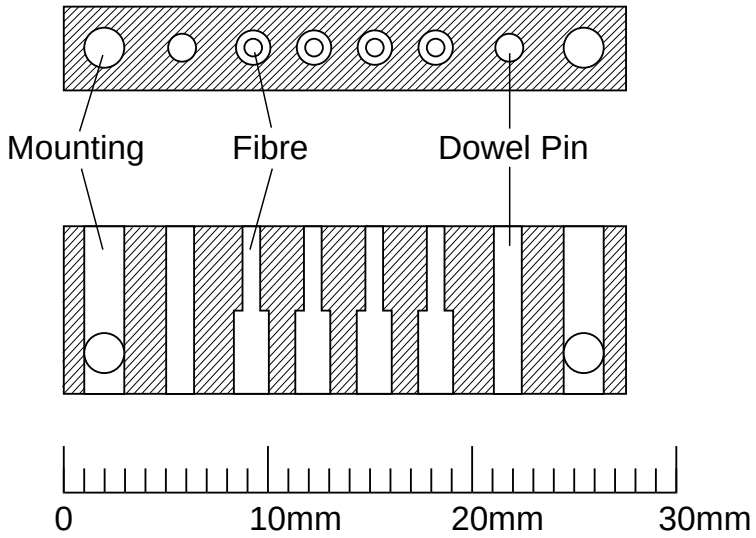

Figure 4: Precision optical connector

Simulation results (see section 4.1, also [18, 27]), confirmed by observations [26], showed that much of the light emerging from the WLS fibres is carried in the outer 20% of their diameter, in helical propagation modes. For good transmission through the

connector, the WLS and clear fibres must therefore be well aligned concentrically, and the mating surfaces must be as flat and close together as possible. In practice, helical modes are suppressed by attenuation as the light passes through the long clear fibre, and the intensity of light arriving at the photomultiplier tube is less sensitive to connector imperfections (such as misalignment and the gap between fibre ends) than might naively be expected. Nevertheless, accurate alignment, surface flatness and reproducibility are important, and careful manufacture, plus precise tightening of the locking screws enabled the connectors to reliably transmit 90% of the light capable of reaching the photomultiplier, with a reproducibility better than 5%. Transmission could be improved using optical grease between the mating surfaces, but this was not done for fear of ageing effects and more difficult reproducibility.

5.4 Photomultiplier Tubes and Couplers

Electron Tubes Ltd. 9902SKA [28], photomultipliers were chosen for their quantum efficiency at 500 nm ($\sim 15\%$), gain ($\sim 2 \times 10^7$), low dark current, cost, size and uniformity of photocathode response [29]. Special tubular housings (QL38) [28] were developed in collaboration with the manufacturer, featuring mu-metal shields at cathode potential, electrostatic and rf shielding, spring loading and positive registration to the Delrin optical coupler (see fig 5), which supports the fibre ends in contact with the photocathode. A hy-

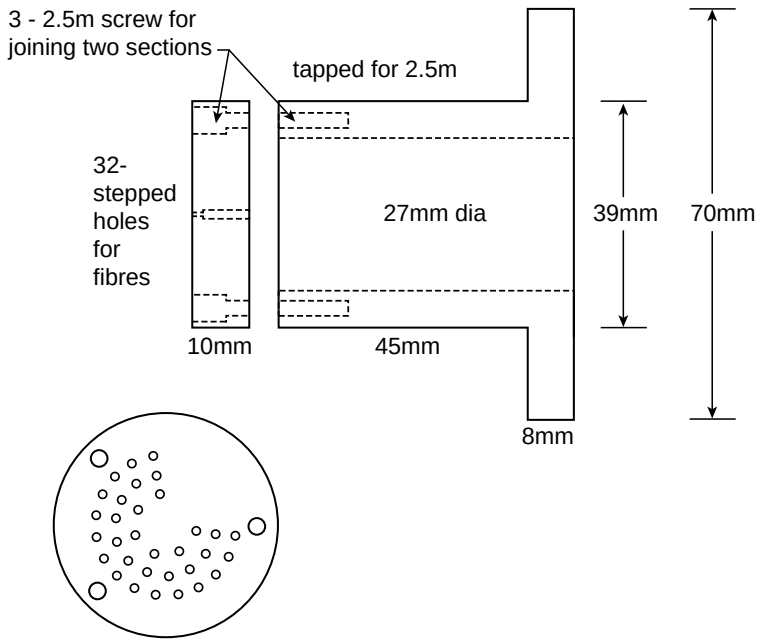

Figure 5: Phototube coupler

drogen annealed soft iron tube surrounding the housing completes the magnetic shielding, to allow operation in the non-uniform fringe field (up to 100G) where the photomultiplier tubes are mounted.

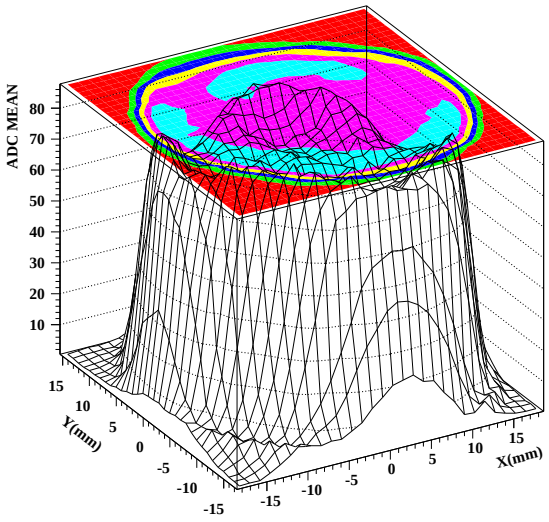

Figure 6: Photocathode uniformity of a 9902SKA photomultiplier

All photomultipliers underwent dark-box acceptance tests [29] whose results were used to adjust the quality control procedures at the production site. The photocathode uniformity was measured using a light source mounted on a computer controlled positioning stage with a step interval of 0.5 mm. The heart of the light source consisted of a piece of WLS fibre illuminated from the side by a blue LED, giving a light spot less than 1.5 mm in diameter at the photocathode. For each point on a 2 mm grid, the number of photoelectrons was determined from a Poisson fit to the charge spectrum recorded by an ADC. Typical results are shown in fig. 6.

The detailed photocathode response information for the first 100 tubes accepted was used to derive an optimum arrangement at the coupler of the 8 fibres from each of the up to four tiles connected to it. Using this arrangement, the maximum non-uniformity in tile-to-tile output, induced by variarions in response across the photocathode, was reduced to less than 6 per cent, regardless of which photomultiplier was selected. This method, exploiting the large number of fibres carrying light from each tile, and the detailed characteristics of the photomultiplier tube, avoids the need to pre-mix the light from different tiles before the photomultipier, minimizing losses and complexity and allowing for simple later expansion of the number of separately read-out tiles.

The gain of each photomultiplier as a function of operating voltage was determined before installation, using a pulsed LED light source. As described in [30] and [14], for low LED intensities, high first stage gain and a sampling time much shorter than the LED on-time per pulse, the gain and n_{pe} values can be approximated from fits to the distribution of output charge as a function of both LED drive voltage and photomultiplier high voltage.

This technique does not require knowledge of the geometry or absolute output of the light source, only that the light output be stable throughout the duration of each test.

It can therefore be repeated as needed after installation, using the LEDs installed in the tiles, and indeed this method was used to equalize the photomultiplier gains. Although the absolute light output of the installed LED's is not needed, each one was nevertheless tested and calibrated before installation to confirm a linear response with applied voltage, and a certain minimum brightness.

5.5 Readout

In the front end readout cards, the raw photomultiplier tube signals pass through Phillips NE5205A amplifiers [31], with part of the output signal being sent to 15-bit CERN CIA ADC's and the other to Analogue Devices AD96685BQ 1 ns comparators [32] with remote threshold control. The discriminated output signals were passed on to 1 ns/count, 16 bit TDCs (Lecroy 2277/3377 [33]) and to a matching module which arranges the signals for input to the OPAL trigger matrix [34, 35]. The trigger matrix combines signals from different subdetectors and forms coincidences in bins of solid angle, from which various combinations can be selected to form an OPAL trigger.

6 Assembly and Quality Control

A process control and data-management framework, based on the World Wide Web, was developed to integrate the data acquisition, analysis, archiving, and retrieval of data obtained from assembly and testing of the various components of the system.

The procedure for testing a completed sector was launched by entering component information on an HTML-based form. These parameters were used by scripts which created command files for the data acquisition on a VME based data acquisition crate. When acquisition was completed, the CERN Physics Analysis Workstation package (PAW, see [36]) was launched to execute the analysis procedure. HTML-based pages were created for the results and links to these web pages were automatically updated on a database home-page.

6.1 Fibres

WLS Fibres were first tested using a DC tungsten halogen light source filtered through a Wratten 47B filter to simulate scintillator light. An optical splitter was used to provide both reference and test signals with the latter being injected at a point in the fibre under test. By comparing light which emerged from the fibre with the reference, defects were readily identified. Only fibre which met an established standard was accepted for use in the looms and this resulted in a rejection rate of approximately 30% overall. The same test was used to check that the fibres of the completed looms were free from serious defects. The cladding of the WLS fibres is very susceptible to crazing and cracking from mechanical stress during all phases of the loom and tile assembly so frequent re-testing was essential to verify optical quality.

Initial test results showed that a particularly simple visual test was effective in finding most of the flaws in the WLS looms. The looms were covered with an opaque sheet so

that only the ends were open to room light. Significant defects showed up as a reduction in the light transmitted from one end to the other and an increase in that backscattered to the same end it entered. This was identifiable by eye through the change in brightness of one end when the other was covered. This simple test was repeated often during the course of the assembly and after completion of the sectors.

The clear fibres were tested using a pulsed light source consisting of WLS fibres emerging from a block of clear plastic, which was excited from the side by blue LEDs. Using a pre-fitted connector, groups of four fibres were coupled to this source at one end, while the the fly-cut, free ends were mated to a photomultiplier tube using a temporary (detachable) coupler. Anode ouput signals were checked for uniformity of response and the fibres were judged acceptable if they transmitted signals that were within 7% of the mean response.

6.2 Tile Sectors

Each scintillator tile was checked for dimensions, surface finish, groove quality and groove depth before gluing. WLS looms were mounted in the grooves using a precision jig to correctly locate the tile and connectors. The pair of WLS fibres from a loom were located and glued one above the other in each groove using either BC 600 or NE581 scintillator cement. Final assembly of the sectors, which is illustrated in fig. 7,

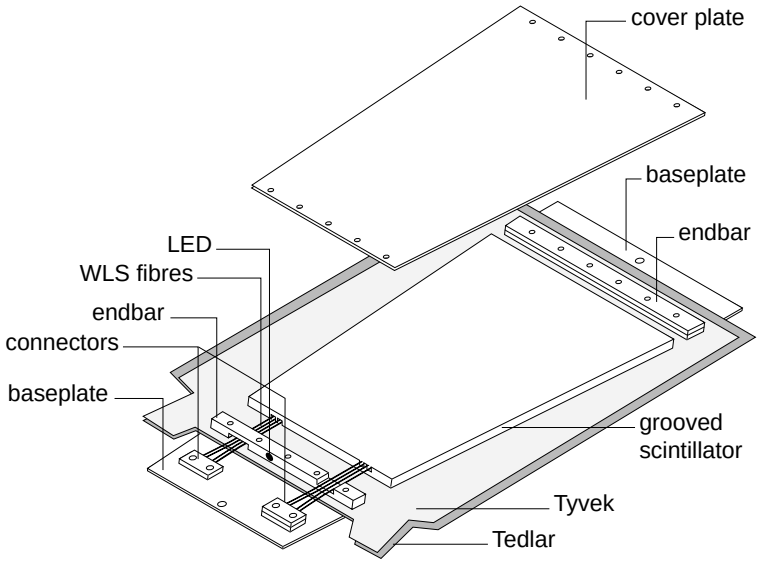

Figure 7: Sector assembly

involved precision placement of the scintillator-fibre units onto backplates, to which 150 μm Tyvek 1073D [21] and 50 μm Tedlar [21] wrapping materials had been pre bonded using 3M 465 2 mil high tack adhesive transfer tape [37]. The Tyvek paper provides high reflectivity and the Tedlar light tightness. The radial edges of neighboring tiles in a plane are separated only by 400 μm of wrapping materials. Endbars bolted to the back

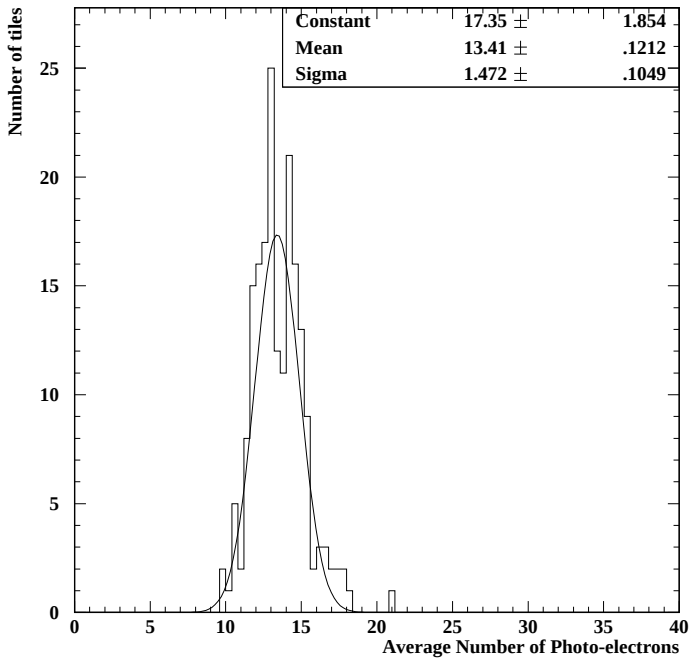

Figure 8: Distribution of mean n_{pe} from cosmic ray events for 196 sectors

and cover plates at the inner and outer radii secured the wrapping and were slotted to allow the fibres to exit. The scintillators were held in place only by the endbars and wrapping materials, while the connectors were bolted to the back plate through oversize holes, allowing some tolerance and avoiding straining the fibres. A pre-calibrated blue LED (CREE Research C470-5D36 [38])was press-fit into a hole in the center of one end bar to illuminate the scintillator for calibration and monitoring. Finally, both ends of the package were light sealed in a two stage process, first with Dow Corning 3145 adhesive sealant [39] and then Sylgard 150 [39].

As soon as wrapping and assembly onto backplates was complete and before sealants were applied, the WLS fibre loops were checked by eye as described above. The LED was pulsed and its function checked by visual verification of the induced WLS fibre output (under darkened conditions). Once a sector package had been completely light-sealed, these simple controls were verified by connection of each WLS fibre end, through standard connectors and 10 m of clear fibre, to a separate photomultiplier tube. The dark count rates of the tubes were compared with previously measured values for any indications of light leaks. The uniformity of response between fibres was then verified by pulsing the LED and fitting the observed charge distributions from each photomultiplier to extract n_{pe}. All fibres were then connected to a single tube operating at a known gain, and the light yield crudely derived from fitting the average charge distribution observed for near vertical cosmic rays, defined by the cosmic ray telescope. The distribution of the average

number of photoelectrons for the first 196 assemblies is shown in fig. 8.

7 Performance

7.1 Beam Test

To validate the overall design, a prototype tile with production optical connectors, clear fibres and photomultiplier, was exposed to beams of electrons, muons and pions in the X5 beamline of the CERN SPS. Details of the apparatus and measurements can be found elsewhere [40]. Fig. 9 shows the tile system response to a normally incident muon beam of approximately 100 GeV. Pedestal events obtained when the beam was absent are also shown and the clear separation between the muon signal and the pedestal peak shows that the light output is sufficient for good efficiency. By fitting this charge distribution, the number of photoelectrons n_{pe} was estimated to be 14.5 ± 1.3, and a uniform efficiency of $\geq 99\%$ was recorded over the tile surface for a 2 photoelectron equivalent threshold.

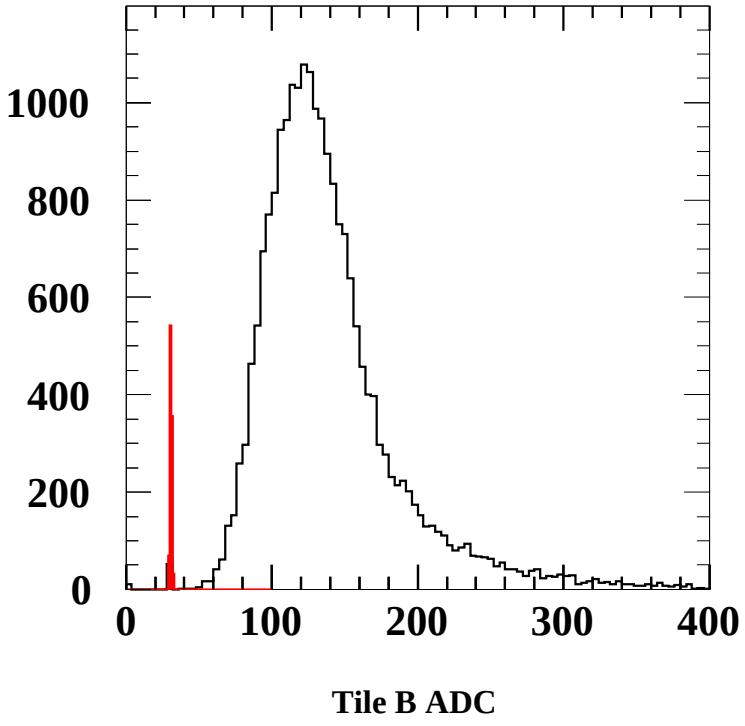

Figure 9: Response of prototype tile to 100 GeV muon beam. The shaded peak on the left is for pedestal events. By fitting the charge distribution, values of 14.5 ± 1.3, and $\geq 99\%$ are obtained for n_{pe} and efficiency respectively for a 2 photoelectron equivalent threshold and normal incidence.

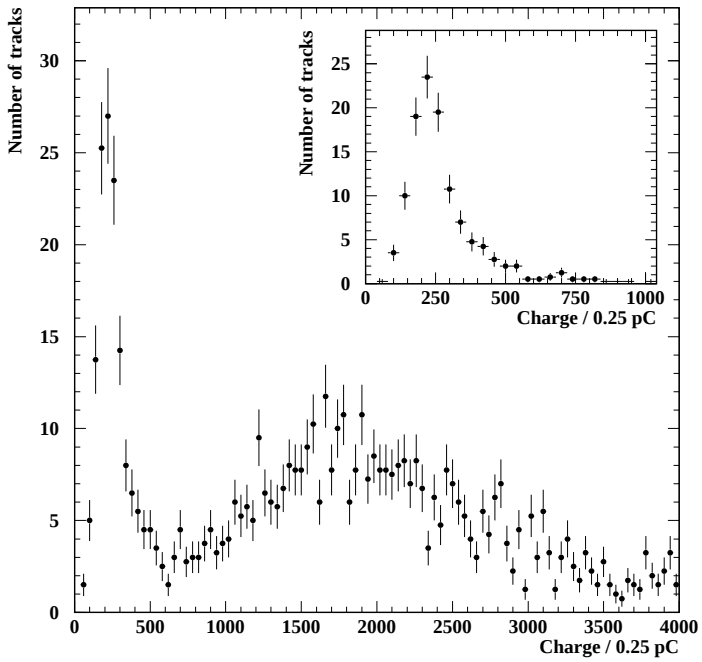

Figure 10: TE charge response to single tracks corrected for angle of incidence and summed over all segments. The inset shows the same spectrum with the condition that the associated electromagnetic calorimeter energy is required to be less than 3 GeV.

7.2 Operation in OPAL at LEP

The uniformity, calibration, efficiency and light yield of the tiles are demonstrated by their response to single tracks from a selection of low multiplicity final states from $e^+e^- \to Z^0$ interactions. Isolated charged particle tracks, with momenta greater than 5 GeV/c, were selected if they projected through any single TE readout segment. The charge (0.25 pC counts) recorded for all such single tracks, corrected for angle of incidence, and summed over all segments, is shown in fig. 10. The broad distribution at higher charges corresponds to electrons which have interacted in the two radiation lengths of material encountered before intersecting the scintillator (see fig.1). The clear minimum ionizing peak is well separated from pedestal and can be isolated (see inset figure) by requiring that each track intercepting a TE tile has an associated electromagnetic calorimeter energy less that 3 GeV. Using a Gaussian fit to the minimum ionizing peak, the light yield was estimated at 14 ± 2 photoelectrons/MIP (a lower limit since any variation in gain for different channels broadens the MIP peak). The same procedure applied to a single channel (with looser selection to increase statistics) yields 15 ± 3 photoelectrons/MIP. These observations highlight the overall uniformity of light yield and the consistency of gain calibration between channels.

Event time distributions for electron-positron collisions at the Z^0, observed during

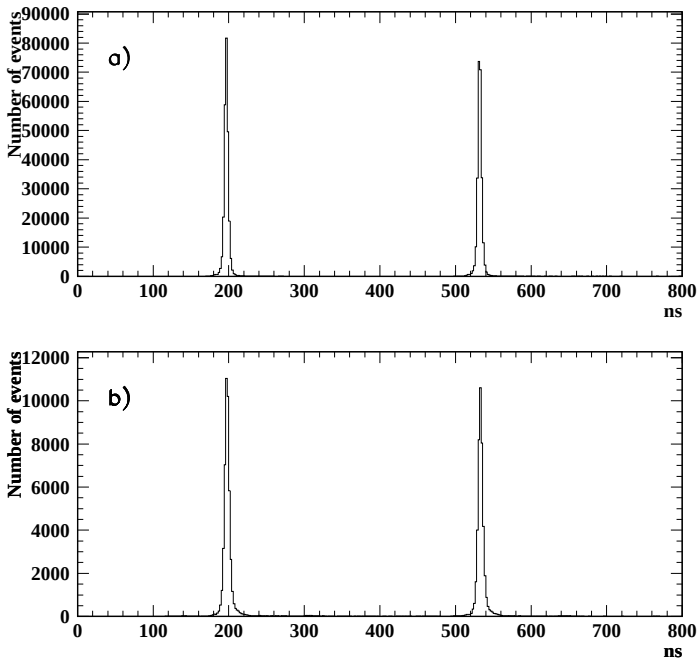

Figure 11: Bunchlets from Z^0 run as seen by MIP Plug tiles (a) and TE tiles (b). The horizontal scale is in ns and the data have been corrected for differences in fibre path lengths, and time slewing due to amplitude variations

bunch train operation with two bunchlets per train, are shown in fig. 11. Data for the small MIP plug tiles around the beam-line are shown in the upper histogram, while the lower one shows the results for larger TE tiles at higher radius. Corrections for differing fibre paths and time slewing have been applied.

The observed spacing between bunches has a mean of 335 ± 1.0 ns (334 ns expected) and a gaussian fit to either bunchlet peak gives sigma = 3.0 ns compared with the design requirement of 5ns. The low noise levels suggested by fig. 11 were confirmed by a study of randomly triggered beam crossings (ie: no physics triggers set). The resulting hit probability per readout channel over the 800 ns active period was found to be $\leq 0.2\%$ in all cases.

8 Conclusion

The OPAL tile-endcap is a successful application of tile-fibre technology, using thin tiles, to the detection of minimum ionizing particles with high efficiency. A time resolution of 3 ns has been achieved, and the measured light yield is 14 photoelectrons/MIP, which results in efficiency of $\geq 99\%$. Experience so far indicates that the detector system is reliable and can be readily calibrated to give uniform response.

9 Acknowledgements

The facilities provided by the team institutes were especially appreciated. The consistent support of R.D. Heuer, D.E. Plane, A.M.Smith and A. Skuja were vital to the successful completion of the project. For initial concepts and the benefit of much accumulated experience, we are indebted to A. Bamberger, A Benvenuti, C. Hearty, J. Freeman, H. Grabosch, P. le Dû, P. Melese, O. Runolfsson and H.Tiecke. The productive partnerships with Bicron Corporation and Electron Tubes Ltd. to customize products for our applications contributed much to the successful completion of the detector system. We gratefully acknowledge the financial support of the following: The Department of Energy, USA, under grant DEFG05-91ER40670, The Natural Sciences and Engineering Research Council of Canada, The Particle Physics and Astronomy Research Council, UK, the Hungarian National Science Foundation (grants T016660, T023479 and F015089) and the Bundesministerium fur Forschung und Technologie.

References

[1] K. Ahmet et al., Nucl. Inst. and Meth. A305(1991)275-319.

[2] W.J. McDonald, Nucl. Phys B. 61B (1998) 366.
A.H. Ball, Proceedings of the Conference on Scintillating and Fibre Detectors, (SciFi 97), Notre Dame, Illinois, to be published.
J.L. Pinfold, Nucl. Phys. B 61B (1998) 83.

[3] V.I. Kryshkin and A.I. Ronzhin, Nucl. Inst. and Meth. A247 (1986) 583.
M.G. Albrow et al., Nucl. Inst. and Meth. A256 (1987) 23.

[4] SDC Collaboration, *Technical Design of a Detector to be operated at the Superconducting Super Collider* SDC-92-201, April 1 1992.

[5] G.W. Foster, J. Freeman and R. Hagstrom, Nucl Phys B, A23 (1991) 93.
P. de Barbaro and A. Bodek, University of Rochester preprint, UR 1398 (1994).
S. Aota et al., Nucl. Inst. and Meth. A352 (1995) 557.

[6] F. Ariztizabal et al.,Nucl. Inst. and Meth. A349 (1994) 384.
Atlas Collaboration, CERN LHCC 97-1 and 97-2, June 1997.

[7] M. Beck et al., Nucl. Inst. and Meth. A355 (1995) 351.

[8] A. Bamberger et al., Nucl. Inst. and Meth. A382 (1996) 419.

[9] A. Benvenuti, (private communication).

[10] B.S. Acharya et al., FERMILAB Pub-97/226-E.

[11] P.de Barbaro et al., Nucl. Inst. and Meth. A315 (1992) 317.

[12] R. Wojcik et al, IEEE Trans Nucl. Sci., 40(1993)4.

[13] T. Asakawa et al., Nucl. Inst. and Meth. A340 (1994) 458.

[14] OPAL technical note TN524 November 25, 1997

[15] S. Bentvelsen, *Semi-analytical simulation of scintillating tiles with WLS fibre readout*, (unpublished).

[16] L. Labarga and E. Ros, Nucl. Inst. and Meth. A249 (1986) 228.

[17] GEANT available from CERN Program Library, Long Writeup W5013 (1994), CERN-CN div., CH 1211 Geneva 23 Switzerland.

[18] C. Hawkes et al., Nucl. Inst. and Meth. A292(1990)329.

[19] Bicron Corp., 12345 Kinsman Rd. Newbury OH 44065 USA

[20] Kuraray Corp., 3-10, Nihonbashi, 2 chome, Chuo-ku, Tokyo 103, Japan.

[21] E. I. duPont di Nemours, Wilminton DE 19898 USA.

[22] NE Technology Ltd., Sighthill, Edinburgh. EH11 4BY Scotland.

[23] Novus Inc., Minneapolis MN 55436 USA.

[24] Hoechst Aktiengesellschaft 65926 Frankfurt am Main, Germany.

[25] Mitsubishi International Corporation, 520 Madison Avenue, New York, NY 10022-4223, USA.

[26] S. Aota et al., Nucl. Inst. and Meth. A357 (1995) 71.

[27] K. H. Able et al., Proceedings of the Workshop on Scintillating and Fibre Detectors, (SciFi 93) Notre Dame, Illinois, World Scientific (1994) 395

[28] Electron Tubes Ltd. (formerly Thorn-EMI), Bury St., Ruislip, Middx HA4 7TA UK.

[29] W. Springer, *Tests of the Hamamatsu R4760 and Thorn-EMI 9902KA Photomultiplier Tubes*, (unpublished).
R. Stubberfield, Electron Tubes Ltd., (private communication).

[30] B. Bencheikh et al., Nucl. Inst. and Meth. A315 (1992) 375.

[31] Philips Components Division, P.O.Box 218, 5600 MD, Eindhoven, Netherlands.

[32] Analog Devices Inc.,One Technology Way, P.O. Box 9106, Norwood, MA 02062-9106, USA.

[33] Lecroy Corp., 700 Chestnut Ridge Road, Chestnut Ridge, NY 10977-6499, USA.

[34] M. Arignon et al., Nucl. Inst. and Meth. A313(1992)103.

[35] M. Arignon et al., Nucl. Inst. and Meth. A333 (1994) 330.

[36] Application Software Group, *Physics Analysis Workstation*,Q121, CERN Program Library, CERN CH-1211 Geneva 23 Switzerland.

[37] 3M Industrial Tape Div., 3M Center, Bldg. 220-7E-01, St. Paul MN55144-1000 USA.

[38] Cree Research, 2810 Meridian Pky., Suite 144, Durham, NC 27713, USA.

[39] Dow Corning Corp., Midland Mich. 48686-0994 USA.

[40] L. A. del Pozo, OPAL Technical Note TN-335.